



Profibrogenic macrophage-targeted delivery of mitochondrial protector via exosome formula for alleviating pulmonary fibrosis

Wei Zhang^{a,1}, Zhuo Wan^{b,1}, Di Qu^{c,d,1}, Wenqi Sun^e, Liang Zhang^e, Yuan Liang^e, Lei Pan^a, Hua Jiang^a, Zichen Ye^f, Mengying Wei^g, Lijun Yuan^e, Guodong Yang^{g,**}, Faguang Jin^{a,*}

^a Department of Pulmonary and Critical Care Medicine, Tangdu Hospital, Fourth Military Medical University, Xi'an, Shaanxi, 710038, China

^b Department of Hematology, Tangdu Hospital, Fourth Military Medical University, Xi'an, Shaanxi, 710038, China

^c Department of Cardiology, Xijing Hospital, Fourth Military Medical University, Xi'an, Shaanxi, 710032, China

^d Department of Clinical Pharmacy, General Hospital of Western Theater Command, Chengdu, Sichuan, 610083, China

^e Department of Ultrasound Diagnostics, Tangdu Hospital, Fourth Military Medical University, Xi'an, Shaanxi, 710038, China

^f Department of Health Service, Health Service Training Base, Fourth Military Medical University, Xi'an, Shaanxi, 710032, China

^g State Key Laboratory of Holistic Integrative Management of Gastrointestinal Cancers, Department of Biochemistry and Molecular Biology, Fourth Military Medical University, Xi'an, Shaanxi, 710032, China

ARTICLE INFO

Keywords:

Pulmonary fibrosis
Macrophages
Mitochondrial fission
Drp1
Exosomes

ABSTRACT

Pulmonary fibrosis (PF) is a devastating lung disease with limited treatment options. During this pathological process, the profibrogenic macrophage subpopulation plays a crucial role, making the characterization of this subpopulation fundamentally important. The present study revealed a positive correlation between pulmonary macrophages with higher mitochondrial mass ($M\phi^{\text{mitohigh}}$) and fibrosis. Among the $M\phi^{\text{mitohigh}}$ subpopulation of $CD206^{+}M2$, characterized by higher expression of dynamin 1-like (*Drp1*), as determined by flow cytometry and RNA-seq analysis, a therapeutic intervention was developed using an exosome-based formula composed of pathfinder and therapeutics. A pathfinder exosome called "exosome^{MMP19} (Exo^{MMP19})", was constructed to display matrix metalloproteinase-19 (MMP19) on the surface to locally break down the excessive extracellular matrix (ECM) in the fibrotic lung. A therapeutic exosome called "exosome^{therapeutics} (Exo^{Tx})", was engineered to display D-mannose on the surface while encapsulating siDrp1 inside. Prior delivery of Exo^{MMP19} degraded excessive ECM and thus paved the way for Exo^{Tx} to be delivered into $M\phi^{\text{mitohigh}}$, where Exo^{Tx} inhibited mitochondrial fission and alleviated PF. This study has not only identified $M\phi^{\text{mitohigh}}$ as profibrotic macrophages but it has also provided a potent strategy to reverse PF via a combination of formulated exosomes.

1. Introduction

PF is characterized by injuries in the lung alveolar epithelium, fibroblastic foci accumulation, progressive ECM, and collagen deposition [1]. To make matters worse, PF has a poor prognosis and limited treatment options [2]. As the cell powerhouse, mitochondria play an essential role in the regulation of signaling, metabolism, and cell death [3]. Mitochondrial dysfunction involves the generation of mitochondrial ROS (mtROS), loss of mitochondrial membrane potential ($\Delta\psi_M$),

reduced ATP synthesis and glutathione levels, as well as the release of mitochondrial DNA [4,5]. Previous studies indicate that mitochondrial dysfunction is emerging as a crucial pathological feature in the development of PF [6–8]. However, the underlying mechanisms of mitochondrial dysfunction in PF remains to be elucidated [9,10].

Macrophages play a critical role in maintaining immune homeostasis and regulating adaptive inflammatory responses. Previous studies have demonstrated that weakened mitochondrial quality control causes mitochondrial dysfunction and metabolic reprogramming in lung

Peer review under responsibility of KeAi Communications Co., Ltd.

* Corresponding author. Department of Pulmonary and Critical Care Medicine, Tangdu Hospital, Fourth Military Medical University, 1st Xinsi Road, Xi'an, Shaanxi, 710038, China.

** Corresponding author. State Key Laboratory of Holistic Integrative Management of Gastrointestinal Cancers, Department of Biochemistry and Molecular Biology, Fourth Military Medical University, 169th Changlexi Road, Xi'an, Shaanxi, 710032, China.

E-mail addresses: yanggd@fmmu.edu.cn (G. Yang), jinfag@fmmu.edu.cn (F. Jin).

¹ Wei Zhang, Zhuo Wan and Di Qu contributed equally to this work.

<https://doi.org/10.1016/j.bioactmat.2023.09.019>

Received 17 March 2023; Received in revised form 24 August 2023; Accepted 25 September 2023

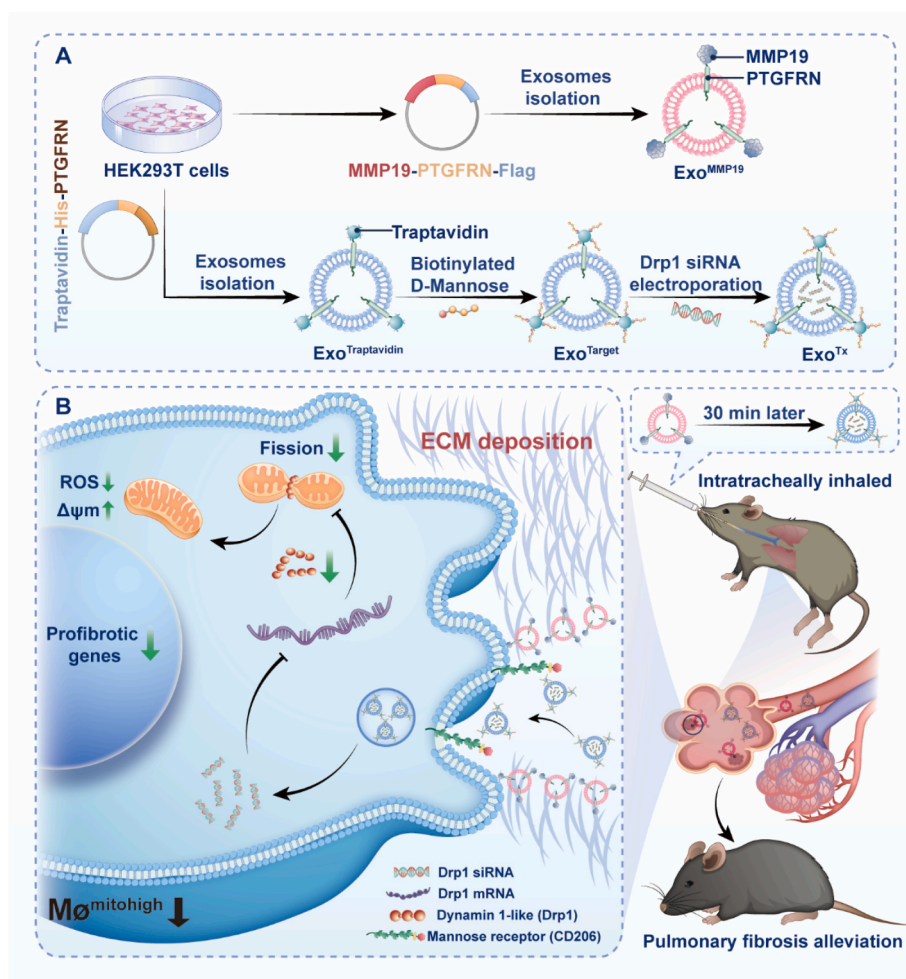
2452-199X/© 2023 The Authors. Publishing services by Elsevier B.V. on behalf of KeAi Communications Co. Ltd. This is an open access article under the CC BY-NC-ND license (<http://creativecommons.org/licenses/by-nc-nd/4.0/>).

macrophages and triggers profibrotic responses [11]. Macrophages in fibrotic lung tissues show abnormalities in mitochondrial mass and the mitochondrial biogenesis process. While the M1/M2 paradigm has been used to understand macrophage polarization, it fails to capture the complexity of macrophage phenotypes in the fibrosis lung [12]. Thus, reclassifying pulmonary macrophage populations based on mitochondrial mass may offer a novel approach to macrophage classification and serve as an appealing therapeutic strategy for treating PF.

Mitochondrial dynamic encompasses two processes: mitochondrial fission and fusion and an imbalance in mitochondrial fission and fusion processes are implicated in the pathogenesis of fibrotic diseases [13,14]. Mitochondrial fission is responsible for regulating the process of mitochondrial fragmentation, controlling the morphology of the mitochondria cristae, and coordinating various processes that require an increased number of fission events [15,16]. Drp1, as the key regulator in the mitochondrial fission process, has been shown to play a central role in several signaling cascades, such as cell differentiation, metabolism, proliferation, and death [17]. It has been reported that mitochondrial fission can boost mtROS production, further disrupt the balance of mitochondrial fusion-fission, aggravate mitochondrial damage, and eventually accelerate the development of PF by polarizing macrophages to a profibrotic phenotype [15,18,19]. Furthermore, lung macrophages isolated from asbestos-exposed mice showed a loss of $\Delta\psi_M$. Drp1

depletion attenuated the loss of $\Delta\psi_M$, while an increase in $\Delta\psi_M$ reduced the production of ROS, subsequently inhibiting fibrosis [20,21]. Given the contribution of profibrogenic macrophages to the pathogenesis of PF by initiating mitochondrial fission, targeting Drp1 may possibly be an appealing therapeutic approach for the treatment of PF.

Exosomes, currently emerging as a rational carrier for drug delivery, are extracellular vesicles ranging from 40 to 150 nm in diameter [22,23]. Previous studies have established exosomes as potential drug carriers for inhalation because of their safety and ability to deliver nucleic acids and proteins to acceptor cells [24,25]. Recently, prostaglandin F2 receptor negative regulator (PTGFRN), a family of type I transmembrane glycoproteins, has been evaluated as a surface display scaffold by fusing an array of structurally and biologically diverse proteins, such as IL-7, IL-12 and CD40L, to the surface-exposed N terminus [26]. In the present study, Exo^{Tx}, a novel kind of therapeutic exosome, was constructed, based on the PTGFRN and biotin-avidin system to treat PF by targeting Drp1 in M₀^{mitohigh}. In addition, given the dense fibrotic stroma in the fibrotic lung, MMP19, a family of endopeptidases that can degrade the ECM in the lung, was delivered to the exosomal surface via the fused protein MMP19-PTGFRN-Flag, allowing MMP19-PTGFRN-Flag-modified exosomes (Exo^{MMP19}) to disrupt the biological barriers and pave the way for Exo^{Tx} delivery (Scheme 1).



Scheme 1. Schematic illustration of the study. Exo^{MMP19}, the pathfinder exosome, and Exo^{Tx}, the therapeutic exosome, were engineered. As prior delivery of Exo^{MMP19} degraded excessive ECM, the way was paved for Exo^{Tx} delivery into M₀^{mitohigh}, the novel profibrogenic macrophage subtype we identified. The formulated exosome therapy inhibited mitochondrial fission and alleviated pulmonary fibrosis efficiently.

2. Results

2.1. Lung macrophage populations can be classified into macrophages with low mitochondrial mass ($M\phi^{\text{mitolow}}$) and macrophages with high mitochondrial mass ($M\phi^{\text{mitohigh}}$)

To elucidate the differences in the mitochondrial mass of lung macrophages, mitochondrial mass was measured in the lungs of wild-type C57BL/6 mice and mice with Bleomycin (BLM)-induced PF (Fig. S1) by flow cytometry. Remarkably, the mitochondrial mass increased in the macrophages of mice with BLM-induced PF (Fig. 1B). Next, lung $M\phi^{\text{mitolow}}$ and $M\phi^{\text{mitohigh}}$ populations in BLM-induced mice were sorted, and the relative mRNA levels of profibrotic cytokines were examined using qRT-PCR (Fig. 1A). The results show that transforming growth factor beta 1 (*Tgf β 1*), platelet derived growth factor alpha (*Pdgfa*), chitinase 3 like 1 (*Chi3l1*), tumor necrosis factor (*Tnfa*), interleukin 1 beta (*IL1 β*), and cellular communication network factor 2 (*Ccn2*) significantly increased in the $M\phi^{\text{mitohigh}}$ compared to $M\phi^{\text{mitolow}}$ (Fig. S2). Furthermore, the expression of M1 specific genes such as *Tnfa*, *IL1 β* and interleukin 12b (*IL12b*) and M2 specific genes such as resistin like alpha (*Retnla*), arginase (*Arg1*) and interleukin 10 (*IL10*) increased remarkably, while M2 specific genes such as interleukin 4 (*IL4*) decreased remarkably in the $M\phi^{\text{mitohigh}}$ in comparison with $M\phi^{\text{mitolow}}$ (Figs. S2 and S3). To explore the mechanism underlying the alteration in mitochondrial mass in BLM-induced PF, $M\phi^{\text{mitolow}}$ and $M\phi^{\text{mitohigh}}$ populations were further sorted for RNA-Seq analysis to compare the gene expression profiles (Fig. 1A). Analysis of differently-expressed genes (DEGs) revealed that 3842 genes were significantly higher in $M\phi^{\text{mitohigh}}$ than in $M\phi^{\text{mitolow}}$ (Fig. 1C). Gene Set Enrichment Analysis (GSEA) showed enrichment in the pathways involved in the positive regulation

of mitochondrial fission, which is significantly involved in the regulation of the mitochondrial mass (Fig. 1D). Furthermore, the expression of various genes was analyzed, including components of the VPS35 retromer complex (*Vps35*), mitochondrial fission genes such as mitochondrial ubiquitin ligase activator of NFKB 1 (*Mul1*), kinase insert domain protein receptor (*Kdr*), mitochondrial elongation factor 1 (*Mief1*), Drp1, DDHD domain containing 1 (*Ddhd1*), DDHD domain containing 2 (*Ddhd2*), and mitochondrial elongation factor 2 (*Mief2*). The results showed a significant upregulation of these genes (Fig. 1E). To validate these findings, qRT-PCR was performed, which validated the fact that Drp1 was the most highly expressed gene in $M\phi^{\text{mitohigh}}$ (Fig. 1F).

2.2. Suppression of *Drp1* could restore mitochondrial dysfunction and decrease expression of fibrotic genes in vitro

To verify the above findings, a cell model was established by exposing bone marrow-derived macrophages (BMDMs) to supernatants derived from mouse lung epithelial-12 (MLE-12) cells treated with BLM/PBS (Fig. S4A). Remarkably, the mRNA levels of *Drp1* in BMDMs were significantly upregulated by the BLM-exposed MLE-12 supernatants (Fig. S4B). Fig. S4C demonstrated that BMDMs treated with supernatants obtained from BLM-exposed MLE-12 exhibited an increase in mitochondrial mass.

Given that mitochondrial dysfunction is characterized by increased mtROS and reduced $\Delta\psi_m$ [27], the alteration in mitochondrial function was examined. Flow cytometry results showed that BMDMs treated with BLM-exposed MLE-12 supernatants had a higher mtROS, reduced JC-1 aggregates and increased JC-1 monomers, indicative of a reduced $\Delta\psi_m$ (Figs. S4D and E). The relative genes expression of *Tgf β 1*, *Pdgfa*, *Chi3l1*, *Tnfa*, *IL1 β* , and *Ccn2* in different groups was then examined. The

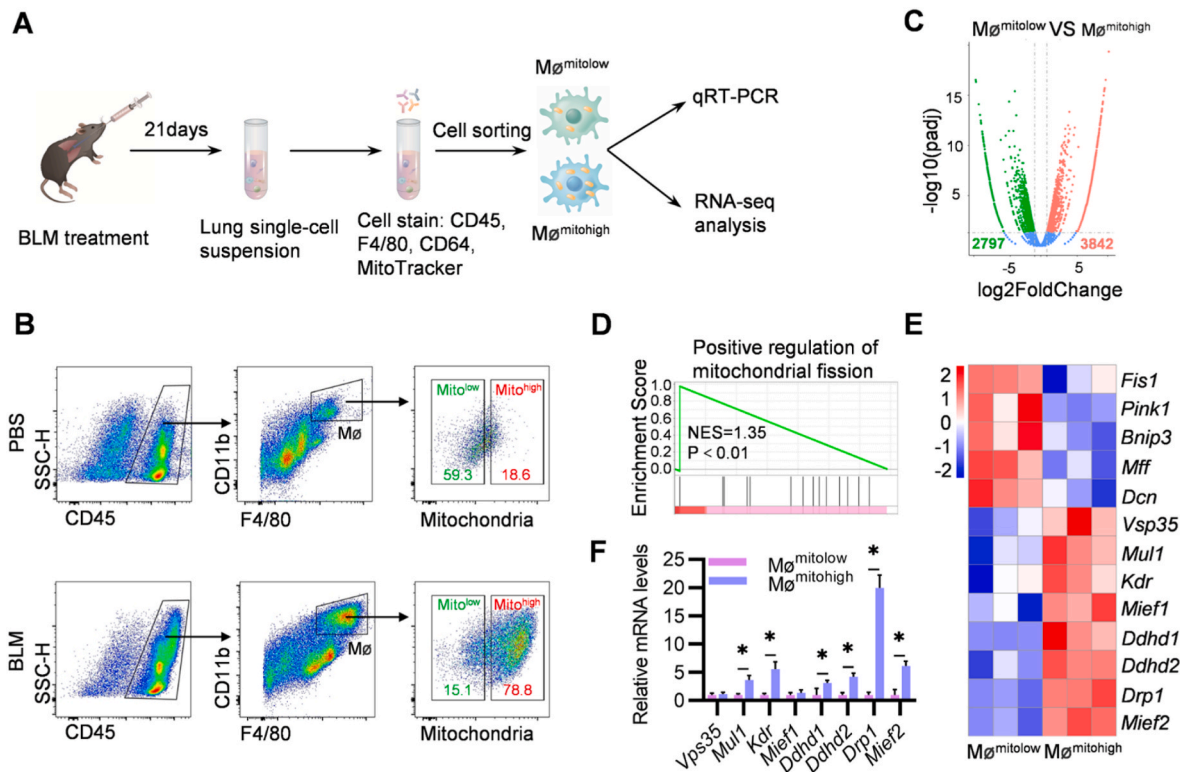


Fig. 1. Drp1 was highly expressed in $M\phi^{\text{mitohigh}}$ of mice with PF. (A) Schematic illustration of the process for RNA-Seq analysis. (B) Flow cytometric analysis of lung Mito^{high} macrophages after intratracheal administration of PBS/BLM. Representative data from three independent experiments. (C) Volcano plot showing DEG between $M\phi^{\text{mitolow}}$ and $M\phi^{\text{mitohigh}}$ in fibrotic lung tissues. (D) GSEA analysis of $M\phi^{\text{mitolow}}$ and $M\phi^{\text{mitohigh}}$. NES, normalized enrichment score. P, Nominal P value. (E) Heat map diagram of mitochondrial fission related genes expression in $M\phi^{\text{mitolow}}$ and $M\phi^{\text{mitohigh}}$. $n = 3$. (F) qRT-PCR analysis of mitochondrial fission related genes in $M\phi^{\text{mitolow}}$ and $M\phi^{\text{mitohigh}}$ in fibrotic lung tissues. Data are expressed as mean ± SEM of three independent experiments. * $p < 0.05$ by two-tailed unpaired Student's t-test.

mRNA levels of these fibrotic genes exhibited a significant increase in the supernatants group when compared to the PBS group (Fig. S4F).

To further elucidate the relation between Drp1 and mitochondrial mass, mitochondrial function, and profibrotic genes, BMDMs were treated with BLM-exposed MLE-12 supernatants and then transfected with siDrp1 for 48 h (Fig. 2A). First, the mRNA and protein levels of Drp1 were analyzed using qRT-PCR and western blotting. The results

revealed that the mRNA and protein levels in the siDrp1 group were significantly lower than those in the PBS and siNC group (Fig. 2B and C). Fig. 2D demonstrates that the siDrp1 group had a lower mitochondrial mass in BMDMs treated with BLM-exposed MLE-12 supernatants. Additionally, siDrp1 also downregulated the mitochondrial mass when BMDMs were treated with PBS (Fig. S5). Next, the role of Drp1 in regulating mtROS and $\Delta\psi_m$ in BMDMs was assessed. In the present

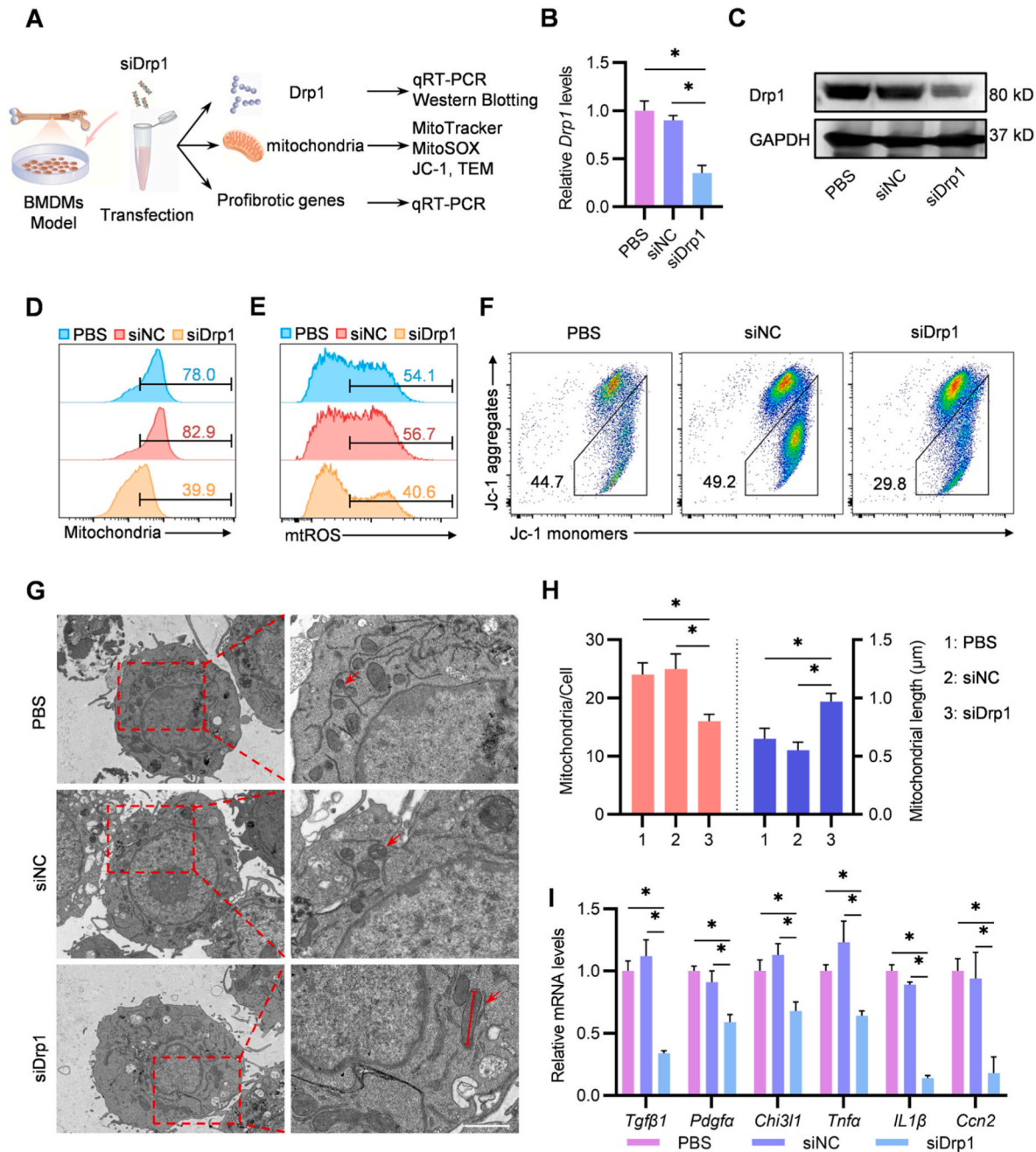


Fig. 2. Interference with Drp1 reversed mitochondrial dysfunction and downregulates profibrotic genes *in vitro*. (A) Schematic illustration of the experiment. BMDMs were transfected with PBS/siNC/siDrp1. (B) qRT-PCR analysis of relative expression of *Drp1* in BMDMs transfected with PBS/siNC/siDrp1. Data are expressed as mean \pm SEM of three independent experiments. $*p < 0.05$ by One-way ANOVA. (C) Western blot analysis of Drp1 expression in BMDMs transfected with PBS/siNC/siDrp1. GAPDH served as the loading control. Representative data from three independent experiments. (D) Flow cytometric analysis of mitochondrial mass in BMDMs transfected with PBS/siNC/siDrp1. Representative data from three independent experiments. (E) Flow cytometric analysis of mtROS in BMDMs transfected with PBS/siNC/siDrp1. Representative data from three independent experiments. (F) Flow cytometric analysis of $\Delta\psi_m$ in BMDMs transfected with PBS/siNC/siDrp1. Representative data from three independent experiments. (G) Representative TEM images of mitochondrial morphology in BMDMs transfected with PBS/siNC/siDrp1. Scale bars: 1 μ m. (H) Calculated mitochondria per cell and mitochondrial length. Data are expressed as mean \pm SEM of three independent experiments in which 30 cells were analyzed. $*p < 0.05$ by One-way ANOVA. (I) qRT-PCR analysis of relative expression of *Tgfb1*, *Pdgfa*, *Chi3l1*, *Tnfa*, *IL1β* and *Ccn2* in BMDMs transfected with PBS/siNC/siDrp1. Data are expressed as mean \pm SEM of three independent experiments. $*p < 0.05$ by One-way ANOVA.

study, it was found that knockdown of Drp1 downregulated mtROS levels while upregulating $\Delta\psi_m$ levels in BMDMs (Fig. 2E and F). Moreover, the morphology of mitochondria was assessed using transmission electron microscopy (TEM), which also found that BMDMs in the siDrp1 group exhibited decreased mitochondria but increased mitochondrial length compared to those in other groups (Fig. 2G and H). Given that *Tgfb1*, *Pdgfa*, *Chi3l1*, *Tnfa*, *IL1 β* and *Ccn2* are significantly involved in PF, in further experiments, whether Drp1 regulated the expression of these fibrotic genes were verified. The results showed that the mRNA levels of these fibrotic genes were significantly down-regulated by siDrp1 compared to the control groups (Fig. 2I). The results above-mentioned indicated that Drp1 played a key role in the regulation of mitochondrial function and expression of profibrotic genes.

2.3. Drp1 was highly expressed in CD206⁺ macrophages

To differentiate the two phenotypically distinct macrophage populations, the differential expression of surface genes between $M\phi^{\text{mitolow}}$ and $M\phi^{\text{mitohigh}}$ was further ascertained by RNA-Seq analysis and qRT-PCR. Fig. 3A, B and S6 demonstrated that among the top 20 highly expressed cell surface genes of $M\phi^{\text{mitohigh}}$ compared to $M\phi^{\text{mitolow}}$, CD206, CD86, CD80, CD163, and CD200R were highly upregulated, and CD206 exhibited the most compellingly increased gene expression compared to others. Next, the correlation between lung CD206⁺ macrophages and $M\phi^{\text{mitohigh}}$ in BLM-induced mice was analyzed (Fig. 3C). Notably, flow

cytometry results showed that mitochondrial mass in CD206⁺ macrophages was much higher than CD206⁻ macrophages (Fig. S7), while CD206⁺ macrophages accounted for the vast majority of the $M\phi^{\text{mitohigh}}$ (Fig. 4D). These findings suggest that, unlike the M1/M2 paradigm, CD206⁺ macrophages may represent the $M\phi^{\text{mitohigh}}$ subset. Given that CD206 and Drp1 surface markers significantly increased in $M\phi^{\text{mitohigh}}$, it was determined whether Drp1 increased in CD206⁺ macrophages (Fig. 3C). By sorting lung CD206⁺ macrophages and CD206⁻ macrophages from mice with BLM-induced PF and measuring their *Drp1* mRNA levels using qRT-PCR, it was found that the level of *Drp1* was higher in CD206⁺ macrophages than in CD206⁻ macrophages (Figs. S8A and B). Drp1 was also found to be overexpressed, as evidenced by the increased fluorescence intensity for CD206⁺ macrophages in the alpha-smooth muscle actin (α -SMA) and collagen type I alpha 1 (Col1a1) double-positive fibrotic lung tissue (Fig. 3E).

2.4. Exo^{Target} can target CD206⁺ macrophages in the lung

According to prior mechanism studies, CD206 may act as a surface marker of the $M\phi^{\text{mitohigh}}$, and Drp1 may play an important role in the regulation of PF. Against this background, Drp1 in CD206⁺ macrophages in the lung were targeted to alleviate PF. In this study, a general and replaceable engineered exosome was constructed for drug delivery, building upon emerging evidence of exosomal potential as drug delivery vehicles [28,29]. First, to generate Exo^{Traptavidin}, we fused the trapta

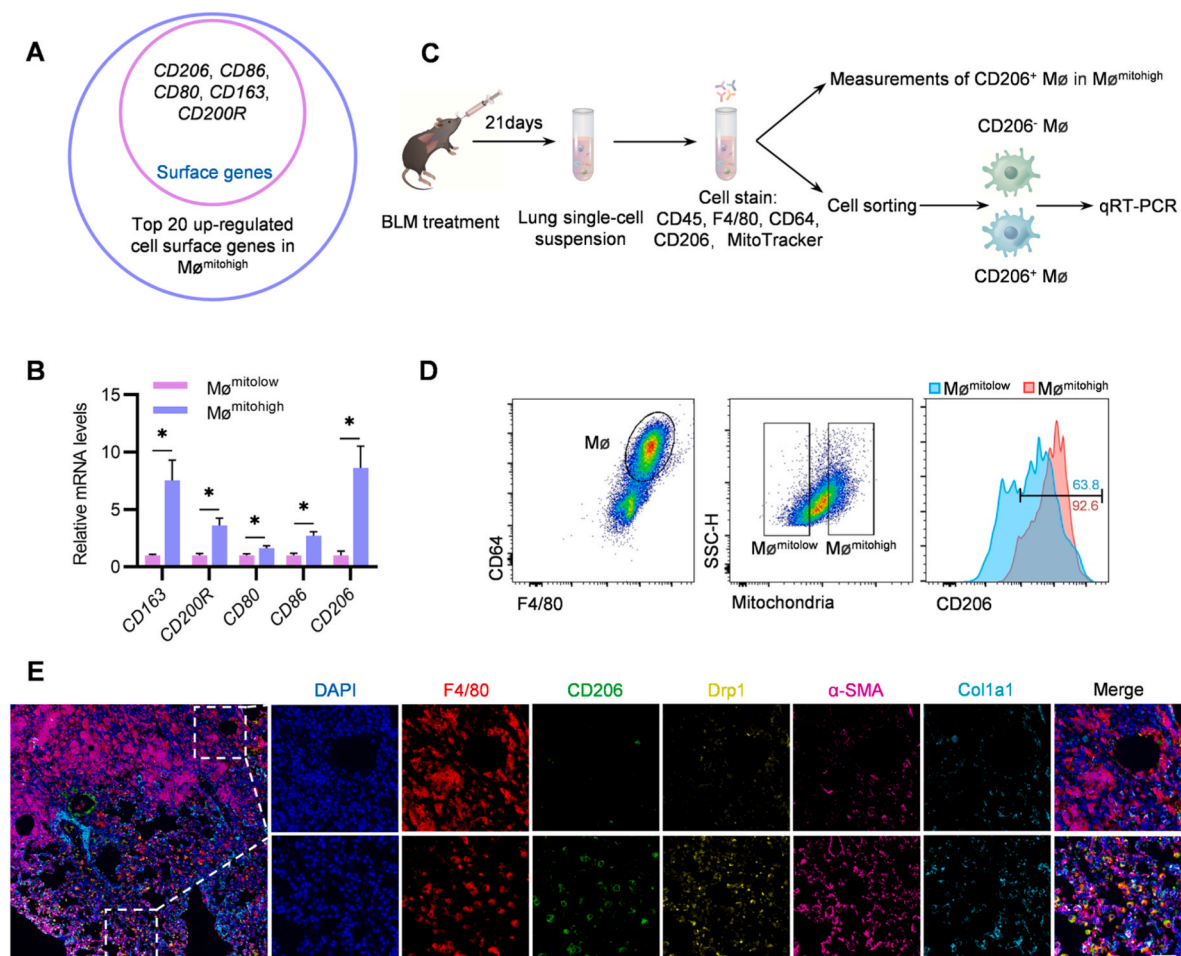


Fig. 3. Drp1 was highly expressed in CD206⁺ macrophages. (A) Venn diagram of highly-expressed cell surface genes of $M\phi^{\text{mitohigh}}$ compared to $M\phi^{\text{mitolow}}$. (B) qRT-PCR analysis of macrophage markers in $M\phi^{\text{mitolow}}$ and $M\phi^{\text{mitohigh}}$ in fibrotic lung tissues. Data are expressed as mean \pm SEM of three independent experiments. * $p < 0.05$ by two-tailed unpaired Student's *t*-test. (C) Schematic illustration of the process for lung flow cytometric analysis and cell sorting. (D) Flow cytometric analysis of mice lung CD206⁺ macrophages in $M\phi^{\text{mitohigh}}$ after BLM-induced PF. Representative data from three independent experiments. (E) Representative multiplexed immunofluorescence images of Drp1 in macrophages of fibrotic lung tissues. Scale bar: 50 μ m. $n = 3$.

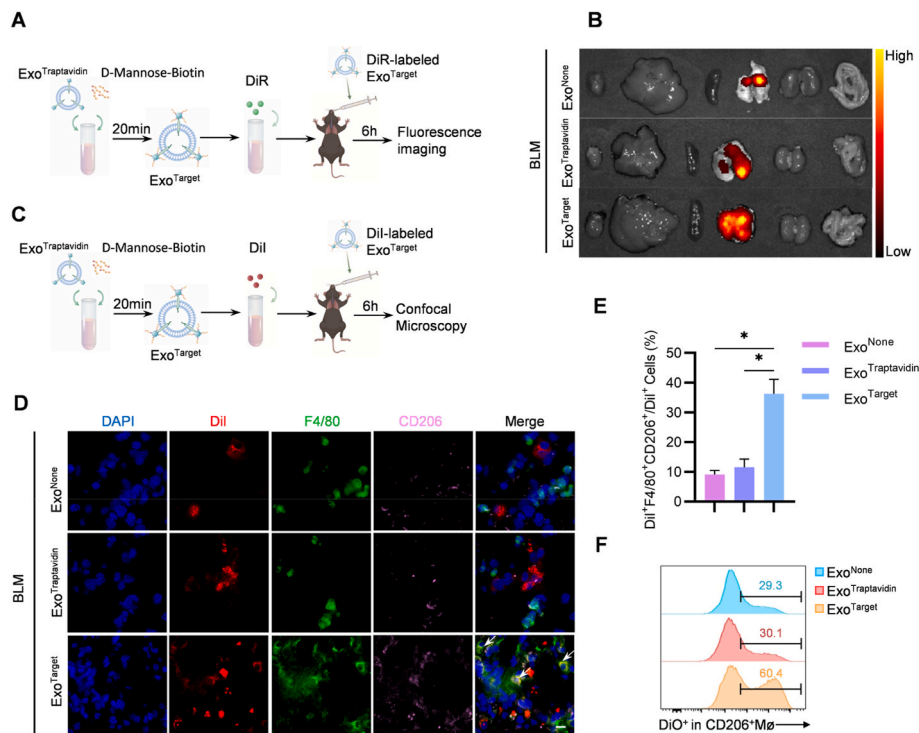


Fig. 4. Exo^{Target} can target CD206⁺ macrophages *in vivo*. (A) Schematic illustration of the experimental procedure. (B) Biodistribution of DiR-labeled Exo^{None}/Exo^{Traptavidin}/Exo^{Target} among organs after the intratracheal administration. $n = 5$. (C) Schematic illustration of the experimental procedure. (D) Representative fluorescence images of the DiI-labeled Exo^{None}/Exo^{Traptavidin}/Exo^{Target} in lung tissues. Scale bar: 10 μm . $n = 5$. (E) The percentage of triple-positive cells in DiI⁺ cells (%). $n = 5$. * $p < 0.05$ by One-way ANOVA. (F) Flow cytometric analysis of DiO⁺ positive CD206⁺ macrophages in fibrotic lung tissues of mice treated with Exo^{None}/Exo^{Traptavidin}/Exo^{Target}. Representative data from five independent experiments.

vidin, a streptavidin variant maximizing biotin binding strength [30], to PTGFRN by introducing the pcDNA3.1(-)-Traptavidin-His-PTGFRN plasmid into human embryonic kidney 293T (HEK293T) cells (Fig. S9A). The supernatants of HEK293T cells to extract exosomes were then collected via ultracentrifugation.

To validate whether the pcDNA3.1(-)-Traptavidin-His-PTGFRN plasmid was successfully transfected into HEK293T cells, western blot analysis was conducted. The results showed overexpression of the Traptavidin-His-PTGFRN fusion protein in both the cells and the derived exosomes (Fig. S9B). A similar increase in the Traptavidin-His-PTGFRN fusion mRNA was also observed in the cells (Fig. S9C). We further analyzed the exosomal inclusive markers (TSG101 and CD9) and the exclusive marker (GM130) by western blot and confirmed that the fusion protein did not change the characteristics of exosomes (Fig. S9D). By TEM (Fig. S9E) and nanoparticle tracking analysis (NTA) (Fig. S9F), it was found that the modification of exosomes did not affect the morphology and size distribution. Moreover, in order to determine whether traptavidin is localized in the extracellular space of exosomes, the engineered exosomes were incubated with biotin-Cy5 antibodies, followed by flow cytometry analysis. The results confirmed that traptavidin was successfully expressed on the surface of Exo^{Traptavidin} (Fig. S9G).

Given that CD206 is the prototypical member of the mannose family of proteins, it is possible for the N-terminal Cysteine-Rich domain of CD206 to bind glycoconjugates terminated in mannose, fucose, or GlcNAc in a calcium-dependent manner [31]. Therefore, Mannose-modified exosomes were developed to specifically target CD206⁺ macrophages. To construct Exo^{Target}, biotinylated D-mannose was bound to Exo^{Traptavidin}. Figs. S10B and C show that Exo^{Target} exhibited a zeta potential of -23.9 ± 2.0 mV and an average size of 129.54 ± 18.34 nm and TEM demonstrated that Exo^{Target} was round-shaped and was enveloped by a membrane with a diameter of approximately 100 nm (Fig. S10A). Next, to assess the *in vivo* distribution of exosomes, DiR dye was

incubated with Exo^{None}, Exo^{Traptavidin}, and Exo^{Target} for 30 min prior to their administration via intratracheal inhalation (Fig. 4A). *In vivo* imaging system (IVIS) showed that both the two control groups and Exo^{Target} accumulated in the lung, whereas Exo^{Target} exhibited higher retention compared to the control groups (Fig. 4B). DiI-labeled exosomes were also tracked through immunofluorescence analysis (Fig. 4C), which revealed that, compared to the controls, Exo^{Target} was localized mainly in the F4/80 and CD206 double-positive cells (Fig. 4D and E). Flow cytometry analysis further demonstrated that Exo^{Target} was specifically targeted to CD206⁺ macrophages (Fig. 4F and S11).

2.5. siDrp1-loaded Exo^{target} (Exo^{Tx}) alleviated mitochondrial dysfunction and suppressed expression of fibrotic genes

In line with the effect of siDrp1 on BMDMs *in vitro*, the mechanism underlying the anti-fibrotic efficacy of Exo^{Tx} was investigated in mice after a BLM induction for 14 days. To address CD206⁺ macrophages in PF mice, Exo^{siNC} and Exo^{Tx} were constructed by loading siDrp1 and siNC into Exo^{Target} via electroporation. As shown in Fig. S12, the encapsulation efficiencies of Exo^{siNC} and Exo^{Tx} were around 0.97 % and 0.92 %, while the loading capacities of Exo^{siNC} and Exo^{Tx} were approximately 52 copies per exosome and 47 copies per exosome, respectively. The zeta-potentials of Exo^{siNC} and Exo^{Tx} were -25.2 ± 2.1 and -25.6 ± 2.3 mV (Fig. S10B), respectively. In addition, TEM (Fig. S10A) and NTA (Fig. S10C) also showed that the siRNA-loaded Exo^{Target} did not change the morphology and size distribution.

Next, BLM-induced mice were forced to intratracheally inhaled with PBS/Exo^{siNC}/Exo^{Tx}. The mitochondrial mass in lung CD206⁺ macrophages of BLM-induced mice was measured using flow cytometry after 48 h. Of note, Exo^{Tx} decreased mitochondrial mass more significantly compared to the PBS and Exo^{siNC} groups (Fig. 5A and S13). Additionally, TEM showed that lung macrophages in the Exo^{Tx} group exhibited less

mitochondria and increased mitochondrial length compared to the controls (Fig. 5B and C). Then, lung CD206⁺ macrophages of BLM-induced mice were sorted by flow cytometry and subjected to qRT-PCR analysis (Fig. 5D). As expected, the results show that Exo^{Tx} significantly downregulated the *Drp1* mRNA (Fig. 5E). Consistent with the effect of siDrp1 *in vitro*, Exo^{Tx} also significantly downregulated the mRNA levels of *Tgfb1*, *Pdgfa*, *Chi3l1*, *Tnfa*, *IL1β*, and *Ccn2* in CD206⁺ macrophages (Fig. 5F). Taken together, results of both *in vitro* and *in vivo* treatment with Exo^{Tx} lend evidence to the observation that suppressing Drp1 in macrophages substantially is a viable approach for the inhibition of fibrotic genes.

2.6. Exo^{MMP19} degraded excessive ECM and served as a pathfinder in the fibrotic lung

Excessive ECM has been acknowledged as a hallmark of PF that blocks the delivery of exosomes to CD206⁺ macrophages, and that MMPs can degrade excessive ECM [32]. However, since some types of MMPs are pro-fibrotic while others have anti-fibrotic functions, such as MMP19 and MMP13 [33]. To degrade excessive ECM in the dense fibrotic stroma without exacerbating the disease progression, Exo^{MMP19} was generated by fusing the MMP19 to PTGFRN through introducing the pcDNA3.1(-)-MMP19-PTGFRN-Flag plasmid into HEK293T cells (Fig. S14A). Consistent with the prior study of characterization of

Exo^{Traptavidin}, western blot (Fig. S14B) and qRT-PCR (Fig. S14C) showed that MMP19-PTGFRN-Flag fusion protein was overexpressed in the cells and exosomes, and exosomes expressed exosomal markers TSG101 and CD9, but did not express the cell-specific marker GM130 (Fig. S14D). TEM (Fig. S14E) and NTA (Fig. S14F) also confirmed that Exo^{MMP19} displayed a typical exosome morphology with a size distribution ranging from 30 to 200 nm in diameter. Moreover, Fig. S14G also revealed that MMP19 is localized in the extracellular space of exosomes by incubating Exo^{MMP19} with FITC-MMP19 antibodies.

In order to determine whether Exo^{MMP19} can degrade the ECM, PBS/Exo^{None}/Exo^{MMP19} was added to the mouse fibroblasts L929 cells (Fig. 6A). Western blot results exhibited that Exo^{MMP19} significantly reduced the expression of fibronectin, Col1a1, and α-SMA of L929 cells (Fig. 6B). Next, to evaluate the *in vivo* distribution of exosomes, DiI-labeled exosomes were inhaled into the lung, the distribution of the DiI-labeled exosomes was measured using IVIS (Fig. 6C). It is noted that Exo^{MMP19} had a stronger ability to accumulate in the lung (Fig. 6D) than controls. DiI-labeled exosomes were then tracked by using immunofluorescence (Fig. 6E), which revealed that Exo^{MMP19} was localized in the less fibrotic area marked by collagen, whereas exosomes of the control groups overlapped with the fibrotic area, indicating Exo^{MMP19} had degraded the excessive collagen (Fig. 6F and G).

Since excessive ECM in fibrotic lungs can prevent exosomes from reaching the fibrotic area, DiI-labeled Exo^{Target} was administered to the

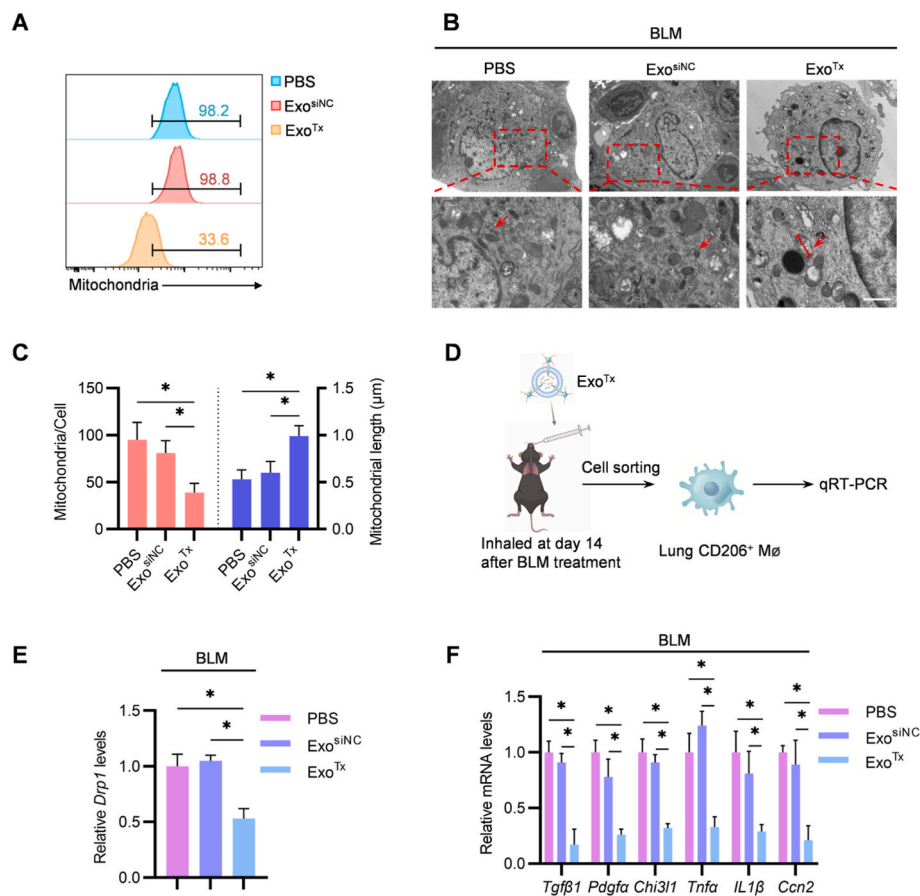


Fig. 5. Exo^{Tx} decreased mitochondrial mass and downregulated the profibrotic genes *in vivo*. (A) Flow cytometric analysis of mitochondrial mass in CD206⁺ macrophages in fibrotic lung tissues of mice treated with PBS/Exo^{siNC}/Exo^{Tx}. Representative data from five independent experiments. (B) Representative TEM images of mitochondrial morphology in lung macrophages treated with PBS/Exo^{siNC}/Exo^{Tx}. Scale bars: 1 μm. (C) Calculated mitochondria per cell and mitochondrial length. Data are expressed as mean ± SEM of five independent experiments in which 50 cells were analyzed. **p* < 0.05 by One-way ANOVA. (D) Schematic illustration of the process for lung cells sorting after exosomes treated. (E) qRT-PCR analysis of *Drp1* in lung CD206⁺ macrophages of BLM-induced mice treated with PBS/Exo^{siNC}/Exo^{Tx}. Data are expressed as mean ± SEM of five independent experiments. **p* < 0.05 by One-way ANOVA. (F) qRT-PCR analysis of *Tgfb1*, *Pdgfa*, *Chi3l1*, *Tnfa*, *IL1β* and *Ccn2* in lung CD206⁺ macrophages of BLM-induced mice treated with PBS/Exo^{siNC}/Exo^{Tx}. Data are expressed as mean ± SEM of five independent experiments. **p* < 0.05 by One-way ANOVA.

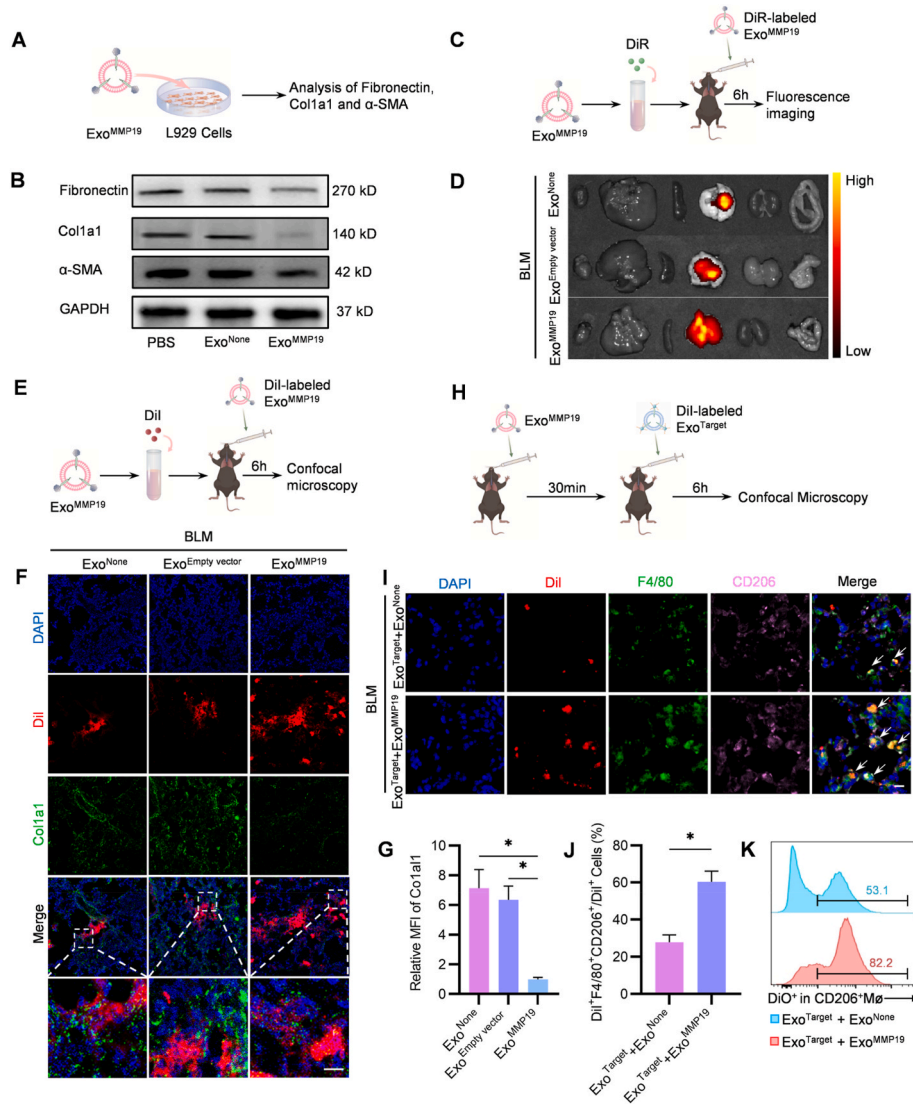


Fig. 6. Exo^{MMP19} degraded excessive ECM and improved the targeting efficacy of Exo^{Target}. (A) Schematic illustration of the experimental procedure. (B) Western blot analysis of fibronectin, Col1a1 and α -SMA of L929 cells. GAPDH served as the loading control. Representative data from three independent experiments. (C) Schematic illustration of the experimental procedure. (D) Biodistribution of DiR-labeled Exo^{None}/Exo^{Empty vector}/Exo^{MMP19} among organs after the intratracheal administration. $n = 5$. (E) Schematic illustration of the experimental procedure. (F) Representative fluorescence images of the DiI-labeled Exo^{None}/Exo^{Empty vector}/Exo^{MMP19} in lung tissues. Scale bar:20 μ m. $n = 5$. (G) Col1a1 relative MFI was analyzed. MFI, mean fluorescence intensity. $n = 5$. $*p < 0.05$ by One-way ANOVA. (H) Schematic illustration of the experimental procedure. (I) Representative fluorescence images of the DiI-labeled Exo^{Target} in lung tissues. Scale bar:10 μ m. $n = 5$. (J) The percentage of triple-positive cells in DiI-positive cells. $n = 5$. $*p < 0.05$ by two-tailed unpaired Student's t-test. (K) Flow cytometric analysis of DiO⁺ CD206⁺ macrophages in fibrotic lung tissues of mice treated with Exo^{Target} + Exo^{None} or Exo^{Target} + Exo^{MMP19}. Representative data from five independent experiments.

BLM-mice 30 min after Exo^{None}/Exo^{MMP19} was inhaled by the mice to evaluate the efficacy of targeting CD206⁺ macrophages (Fig. 6H). As shown in Fig. 6I and J, in the Exo^{Target} + Exo^{MMP19} group, fluorescence intensity of DiI in the F4/80 and CD206 double positive cells remarkably enhanced compared to the group that was treated with the Exo^{Target} + Exo^{None}. Flow cytometry also revealed that Exo^{MMP19} improved the efficacy of Exo^{Target} in targeting CD206⁺ macrophages (Fig. 6K). Taken together, these findings suggest that Exo^{MMP19} can potentially serve as a pathfinder in the treatment of lung fibrosis.

2.7. Intratracheal inhalation of Exo^{MMP19} and Exo^{Tx} alleviated the BLM-induced PF

To illustrate the therapeutic efficacy of engineered exosomes, PF was first induced as described. Then, BLM-induced mice were randomized into six groups treated with PBS, Exo^{None}, Exo^{MMP19}, Exo^{siNC}, Exo^{Tx}, and

Exo^{MMP19} + Exo^{Tx} (30 min after Exo^{MMP19} inhaled), respectively, on days 10, 14 and 17 (Fig. 7A). The alterations of M ϕ ^{mitolow} and M ϕ ^{mitohigh} in lung tissues were first estimated by flow cytometry. Fig. S15 showed that Exo^{Tx} significantly reduced the ratio of M ϕ ^{mitohigh} and Exo^{MMP19} enhanced the effectiveness compared to controls. To verify whether siDrp1 was successfully delivered to CD206⁺ macrophages, lung CD206⁺ macrophages and CD206⁻ macrophages were sorted and the mRNA level of *Drp1* was assessed (Fig. S16A). As shown in Fig. S16B, *Drp1* expression was notably downregulated by the Exo^{Tx} group while Exo^{MMP19} + Exo^{Tx} group exhibited a lower *Drp1* expression in lung CD206⁺ macrophages. However, *Drp1* were only downregulated in the Exo^{MMP19} + Exo^{Tx} group, and there was no significant difference between the Exo^{siNC} and Exo^{Tx} group in the alterations in *Drp1* mRNA in lung CD206⁻ macrophages (Fig. S16C). To further verify the efficacy, immunostaining was applied. Resonating the above findings, Exo^{Tx} remarkably attenuated fluorescence intensity of *Drp1* in lung CD206⁺

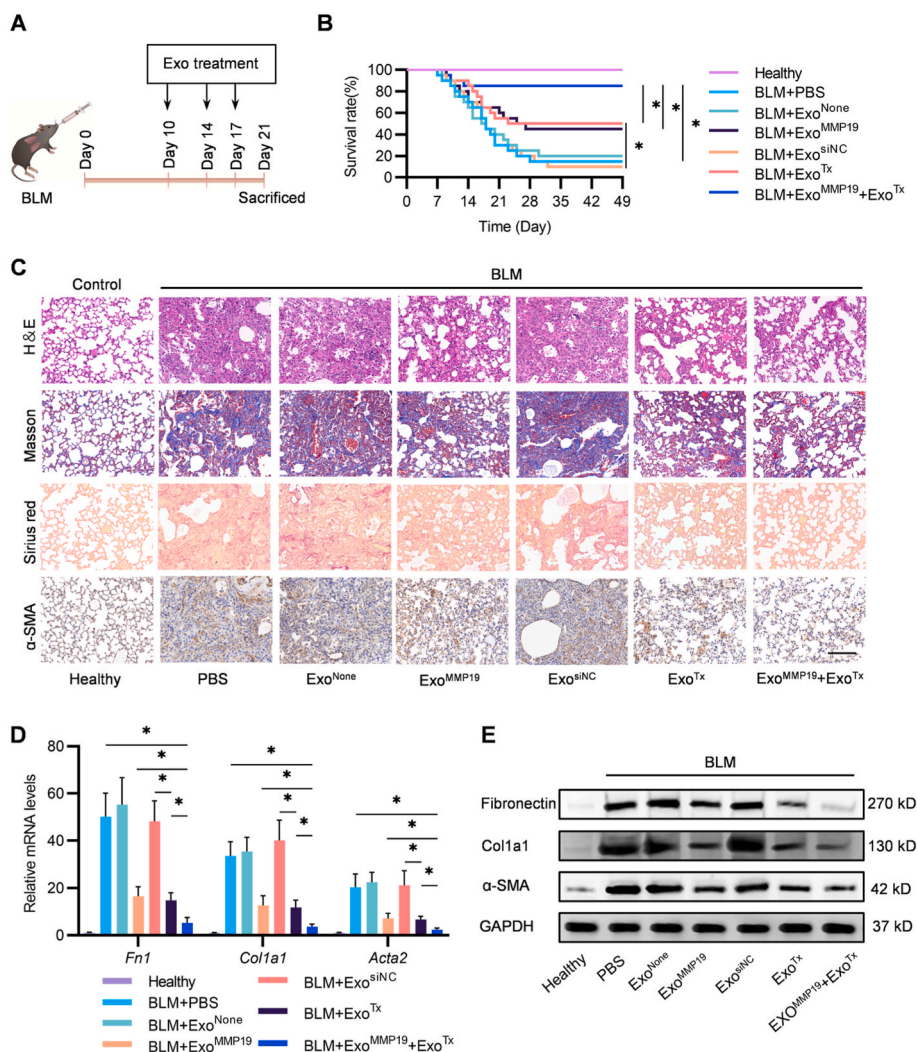


Fig. 7. Therapeutic efficacy of Exo^{Tx} combined with Exo^{MMP19} *in vivo*. (A) Schematic illustration of the experimental procedure and exosomes treatment time course. (B) Survival curve of the mice after treatments. $n = 20$. $*p < 0.05$. (C) Representative H&E, Masson's trichrome, Sirius red staining images and immunohistochemical staining of α -SMA of lung tissues in different groups. Scale bar: 200 μ m. $n = 5$. (D) qRT-PCR analysis of *Fn1*, *Col1a1* and *Acta2* of lung tissues with different treatments. $*p < 0.05$. Data are expressed as mean \pm SEM of five independent experiments. $*p < 0.05$ by One-way ANOVA. (E) Western blot analysis of fibronectin, Col1a1 and α -SMA of lung tissues with different treatments. GAPDH served as the loading control. Representative data from five independent experiments.

macrophages while the Exo^{MMP19} + Exo^{Tx} group exhibited lower fluorescence intensity of Drp1 than other BLM-induced groups (Fig. S16D).

Next, the therapeutic efficacy of targeting Drp1 on PF was assessed. Figs. S17A and B demonstrate that the ROS in lung tissues of the Exo^{Tx} and Exo^{MMP19} + Exo^{Tx} group was notably lower than the controls. Moreover, profibrotic genes *Tgfb1*, *Pdgfa*, *Chi3l1*, *Tnfa*, *IL1 β* , and *Ccn2* in lung tissues of the Exo^{MMP19} + Exo^{Tx} group also remarkably down-regulated compared to the PBS group, and the Exo^{MMP19} + Exo^{Tx} group exhibited a lower mRNA expression of *Tgfb1*, *Pdgfa* and *Ccn2* compared to the Exo^{Tx} group (Fig. S18). To further evaluate the therapeutic efficacy of exosomes, survival rate, western blot, qRT-PCR and immunostaining were conducted to examine the fibrotic markers in the lung. As shown in Fig. 7B, the survival rate of the mice treated with Exo^{MMP19}, Exo^{Tx} and the Exo^{MMP19} + Exo^{Tx} was significantly higher than that of the control groups. However, the Exo^{MMP19} + Exo^{Tx} group exhibited a lower mortality than the Exo^{Tx} or Exo^{MMP19} group. Strikingly attenuated lung injury and fibrosis were also observed in the Exo^{Tx}, Exo^{MMP19} and Exo^{MMP19} + Exo^{Tx} groups as shown by the hematoxylin and eosin (H&E), Masson's trichrome, Sirius red staining, and immunohistochemical staining of α -SMA and the Exo^{MMP19} + Exo^{Tx} group displayed a lower Ashcroft score compared to the Exo^{Tx} or Exo^{MMP19} group. (Fig. 7C

and S19). In good agreement with the above findings, further evaluation of the therapeutic efficacy by qRT-PCR and western blot showed that the mRNA and protein levels of fibronectin (*Fn1*), Col1a1, and α -SMA (*Acta2*) were significantly downregulated in the Exo^{Tx}, Exo^{MMP19} and Exo^{MMP19} + Exo^{Tx} group than in the other PF groups, and Exo^{MMP19} improved the therapeutic efficacy of Exo^{Tx} on alleviating PF. (Fig. 7D and E). To be brief, our data suggest that the formulated exosome combination alleviated the BLM-induced PF more effectively than that treated with Exo^{Tx} only.

3. Discussion

In this study, we reclassified pulmonary macrophages based on mitochondrial mass and validated the role of Drp1 in regulating PF. In addition, a multi-functional drug delivery system was constructed using engineered exosomes to promote a local degradation of ECM and improve mitochondrial function in fibrotic macrophages.

Currently, there are no drugs available that can either improve or stabilize lung function in cases of PF. Inspired by previous studies suggesting that macrophages have augmented mitochondrial mass with increased mitochondrial biogenesis and fission during PF [20,34], we

hypothesized that mitochondrial mass can possibly serve as a novel hallmark for classifying lung macrophage populations in PF. In the present study, pulmonary macrophages were reclassified into two main categories based on mitochondrial mass, viz. $M\phi^{\text{mitolow}}$ and $M\phi^{\text{mitohigh}}$. More importantly, it was observed that the number of $M\phi^{\text{mitohigh}}$ significantly increased whereas that of $M\phi^{\text{mitolow}}$ decreased in BLM-induced mice. In the meantime, $M\phi^{\text{mitohigh}}$ revealed a remarkably high expression of profibrotic genes such as *Tgf β 1*, *Pdgfa*, *Chi3l1*, *Tnfa*, *Il1 β* , and *Ccn2* compared to $M\phi^{\text{mitolow}}$, suggesting that these cells may have the potential to trigger the fibrotic process.

Previous studies have shown that an increase in Drp1 expression can lead to higher mitochondrial mass, fragmented mitochondrial morphology, loose cristae, and reduced $\Delta\psi_m$ [19]. The transcriptome sequencing results in this study also revealed a significant upregulation of Drp1 in $M\phi^{\text{mitohigh}}$, indicating its crucial role in mitochondrial biogenesis and fission and suggesting that Drp1 can potentially serve as a key regulator of mitochondrial fission in PF. Loose cristae and reduced mitochondrial membrane $\Delta\psi_m$ potential may impair mitochondrial electron transport chain, leading to an increase in the levels of mtROS in profibrotic macrophages [35,36]. In the present study, siDrp1 reduced the mitochondrial mass of BMDM models *in vitro* by suppressing mitochondrial fission. At the same time, reduced mitochondrial fission restored the $\Delta\psi_m$, alleviated mtROS generation, and reduced the expression levels of profibrotic genes, including *Tgf β 1*, *Pdgfa*, *Chi3l1*, *Tnfa*, *Il1 β* , and *Ccn2*. These findings suggest that targeting mitochondrial fission could be a potential approach for reversing PF.

CD206⁺ macrophages have been observed in various chronic inflammatory and fibrotic tissue responses [37,38]. Our research also revealed that CD206 mRNA was upregulated compared to CD86, CD80, CD163, and CD200R in the $M\phi^{\text{mitohigh}}$ of BLM-induced lung fibrosis. Thus, our findings strongly support that CD206 can be reliably used as a potential therapeutic target for $M\phi^{\text{mitohigh}}$ in BLM-induced lung fibrosis. A formulated exosome combination system was further constructed to deliver siDrp1 to the $M\phi^{\text{mitohigh}}$ specifically in mice with fibrosis. A general-targeted exosomes were designed by fusing traptavidin with exosomal protein PTGFRN, which has been utilized as a surface display scaffold for structurally and biologically diverse proteins. Biotinylated D-mannose was then mixed with traptavidin expressing exosomes to acquire D-mannose modified exosomes, viz. Exo^{Target}, for CD206 targeting. siDrp1 was loaded into Exo^{Target} and delivered into the fibrotic area. It is noteworthy, however, that siDrp1 decreased the expression level of Drp1 in lung CD206⁺ macrophages. Consistent with the results *in vitro*, Exo^{Target} carrying siDrp1 inhibited mitochondrial fission, restored mitochondrial function, and blunted the release of profibrotic genes in lung CD206⁺ macrophages. Additionally, our CD206-targeting exosomes significantly alleviated lung fibrosis in the BLM-induced mice. Most prior research paid much attention to expressing targeting peptides directly on the surface of exosomes, which results in a narrow range of application [39–41]. In the present study, a traptavidin that expresses exosomes was developed to allow for a free assembly and replacement of proteins on the exosome surface.

In fibrotic lungs, abnormal tissue repair may lead to the proliferation of progressive fibroblast and myofibroblast, causing an excessive deposition of ECM proteins [42], hindering foreign exosomes from reaching alveoli. Notwithstanding the fact that MMPs can degrade ECM proteins, most studies show that MMPs aggravated PF [33]. As MMP-19 protests against PF progression [43], MMP19-PTGFRN-modified exosomes were constructed, referred to as Exo^{MMP19}. These modified exosomes can degrade ECM proteins and facilitate the delivery of CD206-targeting exosomes. The results revealed that Exo^{MMP19} significantly degraded ECM such as fibronectin, Col1a1, and α -SMA. Surprisingly, the confocal images showed that Exo^{Target} had a better target and delivery efficiency combined with Exo^{MMP19}. Furthermore, the combined treatment of Exo^{MMP19} with Exo^{Tx} produced a more pronounced therapeutic efficacy compared to the use of Exo^{Tx} alone. It is worth mentioning that we have applied atomized inhalation instead of the

conventional tail vein administration to deliver exosomes. Since this non-invasive delivery approach is more acceptable to patients, it shows a better efficacy and fewer side effects [44].

4. Limitations of study

A significant relationship between monocyte-derived macrophages and $M\phi^{\text{mitohigh}}$ was not found in according to the RNA-seq data despite that monocyte-derived macrophages are reportedly responsible for fibrotic progression [45]. Moreover, we also did not examine the mitochondrial membrane potential and mitochondrial morphology of $M\phi^{\text{mitolow}}$ and $M\phi^{\text{mitohigh}}$ in lung tissues. This warrants further studies to explore the potential mechanism underlying $M\phi^{\text{mitolow}}$ and $M\phi^{\text{mitohigh}}$ classification.

The process on how Exo^{MMP19} controlled the mRNA expression of Drp1 was not explored in our study. Although there has been scant research on the relationship between MMP19 and Drp1, we speculated that MMP19 reduces intracellular mRNA via the following mechanisms. Characterized by excessive ECM accumulation and ECM stiffening, PF has been reported to correlate with higher levels of Drp1 expression at the mRNA and protein levels in cells cultured on stiff matrix [46]. MMP19, as a kind of matrix metalloproteinases that may alter the characteristics of the ECM by degrading collagen, can affect the expression of Drp1. In addition, it has been reported that ECM can activate macrophages, leading to sustained profibrotic phenotype through enhanced biogenesis and fission processes [15]. Hence, the strategy of reducing extracellular matrix may help alleviate macrophages activation and thereby decrease the level of Drp1. Moreover, it has been reported that MMP19 may be involved in some signaling pathways such as mitogen-activated ERK1/2 pathway and stress-activated JNK and p38 pathways, which are related to mitochondrial dynamics [47,48]. Thus, it is recommended that additional research be conducted to validate the hypothesis stated above.

MMPs, such as MMP19 and MMP13, are anti-fibrotic functions. Hence, Exo^{MMP19} was generated for degrading ECM and thus paved the way for Exo^{Tx} delivery into CD206⁺ macrophages. However, further evaluation is still needed to assess whether other MMPs will be better in degradation of ECMs in PF.

5. Conclusion

In this study, lung macrophage populations were reclassified in BLM-treated mice by mitochondrial mass and found that $M\phi^{\text{mitohigh}}$ contributed to the progression of PF. In terms of mechanism, Drp1 regulated mitochondrial mass, functions, and profibrotic genes. In BLM-induced mice, intratracheal inhalation of Exo^{MMP19} broke down collagen barriers and paved the way for Exo^{Tx} delivery. Additionally, loading Exo^{target} with siRNA against Drp1 significantly inhibited mitochondrial fission, restored mitochondrial functions, and decreased the expression levels of profibrotic genes, ultimately leading to the resolution of PF. Our research has highlighted the critical role of targeting Drp1-mediated mitochondrial fission of $M\phi^{\text{mitohigh}}$ in the protection against PF.

6. Experimental section

6.1. BLM induction of PF and tissue preparation

All male C57BL/6 mice (8–10 weeks) were purchased from Animal Center of the Fourth Military Medical University. The mice were housed in a specific pathogen-free (SPF) animal facility with autoclaved water and irradiated food. All animal experimental procedures were approved by the Animal Experimentation and Ethics Committee of the Fourth Military Medical University (REF NO.20210426-5). C57BL/6 mice were anesthetized with 1 % pentobarbital sodium (50 mg/kg) and then inhaled BLM (5 U/kg, 40 μ l/mouse; Selleck, USA) diluted in PBS or same volume of PBS alone using a microsyringe (YSKD BioTec, China).

To prepare for lung single-cell suspension, mouse lungs were harvested into 5 mL microcentrifuge tube containing 3 ml of 0.5 % collagenase type I (Gibco) at day 21 after BLM inhaled, and then minced into 3–4 mm pieces. After 2 h of incubation at 37 °C, the tissues were filtered through a nylon mesh into a 15 ml centrifuge tube and washed 2 times by centrifugation (1400 rpm, 5 min, 4 °C) in cell stain buffer (BioLegend). The cells were then lysed by resuspending cell pellet in 500 µL of RBC lysis buffer (eBioscience) for 15 min at 4 °C. After centrifugation (1000 rpm, 5 min, 4 °C) and washing with cell stain buffer (1000 rpm, 5 min, 4 °C), cells were counted under the microscope for cell stain.

6.2. Flow cytometry

For flow cytometry and cell sorting, cells were blocked by TruStain FcX™ PLUS Antibody (BioLegend) and then incubated with Fixable Dead Cell Stain Near-IR fluorescent exclude dead cells (Life Technologies) on ice for 20 min. Cells were then stained with the following antibodies: CD45-BV421 (BioLegend), F4/80-PE/Dazzle™594 (BioLegend), CD64-PE/Cyanine7 (BioLegend), CD206-APC (BioLegend), mitochondria-MitoTracker™ Green (Invitrogen), mtROS-MitoSOX™ Red (Invitrogen) and MMP-eBioscience™ JC-1 (Invitrogen). Subsequently, they were washed twice with cell stain buffer. After the final washing, the cell population was sorted in a BD FACSAria II flow cytometer (BD Biosciences, USA) or performed by the NovoCyt D1040 (ACEA Biosciences, USA) or CytoFLEX (Beckman Coulter, USA). The data were further analyzed with FlowJo 10.8.1 software.

6.3. RNA sequencing (RNA-seq)

RNA-Seq was conducted by Novogene Cp. Ltd (Beijing, China). Total RNA from the sorted lung CD45⁺F4/80⁺CD64⁺mito^{low} cells and CD45⁺F4/80⁺CD64⁺mito^{high} of BLM-treated mice was extracted by Trizol reagent. Following the manufacturer's recommendations, sequencing libraries were generated according to NEBNext® Ultra™ RNA Library Prep Kit for Illumina® (New England Biolabs, USA). The library preparations were sequenced on an Illumina HiSeq platform, and 125 bp/150 bp paired-end reads were generated. Three biological replicates were used for each group.

6.4. Cell culture

MLE-12 were purchased from the American Type Culture Collection (ATCC) and were cultured in DMEM/F12 (Gibco) supplemented with HEPES (25 mM, Gibco), pyruvate (1 mM, Gibco), amphotericin B (0.25 g/ml, Gibco), 1 % penicillin/streptomycin (Gibco), and 10 % fetal bovine serum. 10⁷ cells were seeded into a 10 cm dish, exposed to BLM (100 mU/ml) or PBS for 24 h, and then supernatants were collected for further use.

The isolation and culture of BMDMs were performed according to the protocol of Zhang et al. [49]. The hind legs were amputated from the rest of the body, and the muscles surrounding the tibia and femur were dissected. Working in the DMEM (Gibco) supplemented with 10 % fetal bovine serum and 1 % penicillin/streptomycin, the ends of bones were cut off and then flushed with sterile PBS in a 10 cm dish. The progenitor cells were centrifuged at 1000 rpm for 5 min, and then the supernatant was discarded. Next, cells were resuspended and seeded on a 10 cm dish with bone marrow macrophage complete medium DMEM supplemented with 10 % fetal bovine serum, 1 % penicillin/streptomycin, and 20 ng/ml M-CSF (Sino Biological Inc, China). After 7 days of differentiation at 37 °C, 5 % CO₂ incubator, cells were seeded into 6-well dishes, exposed to supernatants (1:1) from MLE-12 treated with BLM or PBS for 24 h, and then cells were collected for further experiments.

HEK293T cells were purchased from Procell Biotechnology and cultured in complete media containing high glucose DMEM supplemented with 10 % fetal bovine serum and 1 % penicillin/streptomycin in a humidified incubator with 5 % CO₂ at 37 °C.

The mouse fibroblasts L929, obtained from ATCC, were cultured in RPMI 1640 (Gibco) supplemented with 10 % fetal bovine serum, and 1 % penicillin/streptomycin in a humidified incubator with 5 % CO₂ at 37 °C. Cells were seeded (10⁶ cells/well) into 6-well dishes. PBS, Exo^{None} or Exo^{MMP19} (at a protein level of about 1 mg/mL) were added to the well and co-incubated for 12 h. Cells were then collected for further use.

6.5. Plasmid construction

Using pcDNA3.1 (–) as the vector, the Traptavidin-His-PTGFRN fragment, and MMP19-PTGFRN-Flag fragment were respectively inserted into the downstream of the promoter cytomegalovirus to construct expression vectors. The gene synthesis and vector construction were synthesized by Genscript Biotech Corporation (GenScript, China).

6.6. Exosome isolation and characterization

Exosomes were collected from HEK293T cells and purified using an ultrafiltration method. HEK293T cells were cultured for 48 h in serum-free DMEM before collection. Next, the supernatants were collected and centrifuged at 3000 g for 15 min to remove dead cells and cellular debris and filtered with a 0.22 µm filter. Then the supernatants were centrifuged at 100,000 g for 70 min at 4 °C. Exosomes were then washed and resuspended in sterile PBS and stored at –80 °C for further experiments. For TEM analysis, exosomes were added to the grid and stained with 2 % uranyl acetate and imaged by TEM (JEM-2000EX and JEM-1400FLASH, JEOL, Japan). For NTA, the isolated exosomes were diluted to 1 mg/mL and analyzed by NanoPlus (Otsuka Electronics, Japan). The zeta potential of exosomes was measured by dynamic light scattering (Malvern Zetasizer, UK). The size distribution and zeta potential of exosomes are listed in Table S2.

6.7. Exosome labeling and tracking in vivo

For *in vivo* analysis of distribution of exosomes, exosomes (about 1 mg/mL at protein level) were incubated with 1 mM DiR (Invitrogen), DiI (Invitrogen) or DiO (Invitrogen) at a ratio of (500:1 in volume) for 30 min at 37 °C. Free dyes were then removed by washing with PBS. DiR-labeled exosomes were intratracheally inhaled via a microsyringe. The distribution of exosomes was analyzed by an IVIS Lumina II *in vivo* imaging system (PerkinElmer, Thermo Fisher, USA) after 6 h. For analysis of the intercellular and intracellular distribution of exosomes, mice were forced to intratracheally inhale with DiI-labeled exosomes via a microsyringe. After 6 h, mice were sacrificed and their lungs were isolated. The isolated lungs were fixed for 15 min with 4 % paraformaldehyde before sectioning. The fresh lung tissue was then embedded in an optimal cutting temperature compound and sectioned at a thickness of 8 µm. After being blocked with 5 % bovine serum albumin (BSA) for 1 h, the tissue sections were incubated with anti-F4/80 (Proteintech, 28463-1-AP, 1:500), and anti-CD206 (Proteintech, 60143-1-Ig, 1:500) or anti-collagen I (Abcam, ab21286, 1:200) overnight. Next, the tissue sections were incubated with FITC goat anti-rabbit IgG antibody (Proteintech, SA00003-2, 1:100) or CoraLite647 donkey anti-mouse IgG antibody (Proteintech, SA00014-8, 1:100) at room temperature for 1 h. The nuclei were counterstained with 4'-6-diamidino-2-phenylindole (DAPI) (Invitrogen). The DiI-labeled exosomes were tracked in a fluorescence microscope (ECLIPSE Ti, Nikon, Japan). To analyze the target efficacy of exosomes, DiO-labeled exosomes were intratracheally inhaled via the microsyringe. After 6 h, mice were sacrificed, and lung single-cell suspension was prepared for flow cytometry.

6.8. Preparation of siRNA-loaded exosomes (Exo^{Tx})

To generate Exo^{Tx}, siDrp1 was added into Exo^{Target} by electroporation. Briefly, Exo^{Target} was firstly prepared by incubating Exo^{Traptavidin} with biotinylated D-Mannose (0.1 mg, QIYUE) in PBS for 20 min. Next,

siRNA was added to the mixture at a final concentration of siRNA: exosome protein = 0.5OD:200 µg. Electroporation was then performed at 700V, 150 µF for 2 pulses in 0.4 cm electroporation cuvettes. To calculate the encapsulation efficiency and loading efficiency of siRNA, exosomes were diluted with PBS and then centrifuged at 100,000×g for 70 min to remove free siRNA. The RNA was isolated from pellets using Trizol reagent according to the manufacturer. The copy numbers were calculated via an absolute RNA quantification method. The standard curves that created by serial dilution of purified and quantified PCR products of each synthesized siRNA. Exosome particle numbers were obtained by NTA. The encapsulation efficiency and loading capacity of siRNA was calculated using the following formulas:

$$\text{Encapsulation efficiency (\%)} = \frac{\text{loaded siRNA}}{\text{original siRNA}} * 100\%$$

$$\text{Loading capacity} = \frac{\text{copies of loaded siRNA}}{\text{number of exosomes}} * 100\%$$

6.9. Animal experiments

The specific grouping of the experiment animals is as follows: (1) Healthy group: PBS + PBS; (2) BLM model: BLM + PBS; (3) Exosomes control group: BLM + Exo^{None}; (4) Exo^{Target} control group: BLM + Exo^{siNC}; (5) Exo^{Target} group: BLM + Exo^{Tx}; (6) Exo^{MMP19} group: BLM + Exo^{MMP19}; and (6) Exo^{MMP19} + Exo^{Tx} group (1:1): BLM + Exo^{MMP19} + Exo^{Tx}. On days 10, 14, and 17 following BLM induction, exosomes (0.5 OD siRNA/200 µg exosomes per mouse) were administered to the corresponding group of mice. All the mice were euthanized on day 21 following the BLM challenge to analyze PF.

6.10. Histology

Mice were sacrificed and perfused with PBS; thereafter, the lungs were collected and fixed in 4 % PFA for further use. Immunofluorescence staining was performed on paraffin-embedded tissue slices followed by permeabilization and blocking with 5 % BSA. The antibodies used for staining included anti-F4/80 (Abcam, ab6640, 1:100), anti-CD206 (Proteintech, 60143-1-Ig, 1:500), and anti-Drp1 (Proteintech, 12957-1-AP, 1:300). Alexa Fluor 488 anti-mouse IgG antibody (Invitrogen, A-11001, 1:200), Alexa Fluor 594 anti-Rat IgG antibody (Invitrogen, A-21209, 1:200), and Alexa Fluor Plus 647 anti-rabbit IgG antibody (Invitrogen, A32733, 1:200) were used as fluorescent secondary antibodies. The ROS content in lung tissues was determined using ROS-specific fluorescent staining [50]. Fresh lung tissues were collected and stained with ROS-specific fluorescent dihydroethidium (DHE). The nuclei were counterstained with DAPI. Images were observed using a fluorescence microscope. Lung and tissue samples from BLM-induced mice were evaluated by H&E, Masson's trichrome, and Sirius red staining. H&E stained sections were used for Ashcroft scoring, performed in a design-blind way. The expression of α-SMA (Abcam, ab5694, 1:200) in the lung was evaluated by immunohistochemistry.

6.11. Multiplexed immunofluorescence (mIF) staining

mIF staining was conducted using the PANO 7-plex immunohistochemistry kit, cat 0004100100 (Panovue, China). Formalin-fixed and paraffin-embedded (FFPE) lung tissue blocks were consecutively sectioned into 5 µm sections. Then the FFPE tissue slides were incubated consecutively with primary antibodies F4/80 (CST, 70076, 1:200), CD206 (CST, 24595, 1:200), Drp1 (Abcam, ab184247, 1:200), α-SMA (Abcam, ab5694, 1:200), and Col1a1 (Abcam, ab21286, 1:200). This was followed by incubation with horseradish peroxidase-conjugated secondary antibody incubation and tyramide signal amplification. The nuclei acids were stained with DAPI. Multiplexed stained sections were imaged using an Olympus VS200 (Olympus, Germany), in conjunction

with Olympus UPLXAPO 20x objective lens. Multilayer images were annotated using QuPath software.

6.12. Quantitative Real-time PCR

Total RNA was isolated from tissues, cells, or exosomes by Trizol (Invitrogen) according to the manufacturer's instructions. PrimeScript First-Strand cDNA Synthesis Kit (Takara) was used for total RNA reverse transcription. The RNA quantity and quality were measured with a NanoDrop 2000 spectrophotometer (Thermo Scientific, USA). qRT-PCR was performed on a Roche LightCycler 96 qPCR system (Roche) using SYBR Green Mix (Takara). RNA expression was normalized to GAPDH levels and calculated using $2^{-\Delta\Delta Ct}$. The primer sequences are listed in Table S1.

6.13. Western blotting

Tissues, cells, or exosomes were subjected to RIPA lysis buffer (Beyotime). Purified proteins were separated in 8 % or 12 % SDS-PAGE and then transferred onto a nitrocellulose membrane, which was blocked with 5 % BSA for 1 h, and incubated overnight with primary antibodies at 4 °C.

The primary antibodies used included anti-Fibronectin (1:1000, Abcam, ab2413), anti-Col1a1 (1:1000, Invitrogen, PA5-29569), anti-α-SMA (1:1000, Abcam, ab5694), anti-Drp1 (1:1000, Proteintech, 12957-1-AP), anti-GM130 (1:1000, Abcam, ab30637), anti-TSG101 (1:500, Santa, sc-7964), anti-CD9 (1:1000, Proteintech, 20597-1-AP), anti-His (1:1000, Proteintech, 66005-1-Ig), anti-PTGFRN (1:1000, Abcam, ab97567), anti-Traptavidin (1:1000, Prospec, ANT-345), anti-Flag (1:1000, Proteintech, 20543-1-AP), anti-MMP19 (1:1000, Proteintech, 14244-1-AP), and anti-GAPDH (1:5000, Abcam, ab181602). Secondary antibodies used in the study included HRP Conjugated goat anti-mouse IgG (1:5000, Proteintech, SA00001-1) and HRP Conjugated goat anti-rabbit IgG (1:5000, Proteintech, SA00001-2). The bands were visualized using the ECL Prime Western Blotting Detection Reagent (GE Healthcare, UK).

6.14. Statistical analysis

All statistics were analyzed using GraphPad Prism 9. Experimental data in this study are expressed as mean ± SEM as indicated. Two-tailed unpaired Student's t-test was used for two groups comparison while a one-way ANOVA test was used to compare the differences across more than three groups. The significance for survival was analyzed by using Kaplan–Meier with log-rank analysis. A *p* value < 0.05 indicates statistical difference.

Ethics approval

All animal experimental procedures were approved by the Animal Experimentation and Ethics Committee of the Fourth Military Medical University (REF NO.20210426-5).

We confirm we have complied with all relevant ethical regulations for animal testing and research, as detailed in the methods.

CRediT authorship contribution statement

Wei Zhang: Conceptualization, Methodology, Validation, Writing – original draft. **Zhuo Wan:** Conceptualization, Methodology, Investigation. **Di Qu:** Methodology, Investigation. **Liang Zhang:** Validation. **Yuan Liang:** Investigation. **Lei Pan:** Conceptualization, Supervision. **Hua Jiang:** Methodology. **Mengying Wei:** Validation, Investigation. **Lijun Yuan:** Supervision, Validation, Investigation. **Guodong Yang:** Conceptualization, Supervision, Writing - review & editing. **Faguang Jin:** Conceptualization, Funding acquisition, Supervision, Validation.

Declaration of competing interest

The authors declare that they have no known competing financial interests or personal relationships that could have appeared to influence the work reported in this paper.

Acknowledgements

Wei Zhang, Zhuo Wan, Di Qu contributed equally to this work. This study was supported by the National Natural Science Foundation of China (Grant Nos. NSFC 81970076) and Key R&D Program of Shaanxi Province, China (2022ZDLSF01-10)

Appendix A. Supplementary data

Supplementary data to this article can be found online at <https://doi.org/10.1016/j.bioactmat.2023.09.019>.

References

- M. Selman, A. Pardo, Idiopathic pulmonary fibrosis: an epithelial/fibroblastic cross-talk disorder, *Respir. Res.* 3 (2002) 3.
- B. Ley, H.R. Collard, T.E. King Jr., Clinical course and prediction of survival in idiopathic pulmonary fibrosis, *Am. J. Respir. Crit. Care Med.* 183 (4) (2011) 431–440.
- A.J. Roger, S.A. Munoz-Gomez, R. Kamikawa, The origin and diversification of mitochondria, *Curr. Biol.* 27 (21) (2017) R1177–R1192.
- Y. Wang, N. Li, X. Zhang, T. Horng, Mitochondrial metabolism regulates macrophage biology, *J. Biol. Chem.* 297 (1) (2021), 100904.
- Q. Xiong, X. Tian, C. Xu, B. Ma, W. Li, Y. Xia, W. Liu, B. Sun, Q. Ru, X. Shu, Mediation of PM2.5-induced cytotoxicity: the role of P2X7 receptor in NR8383 cells, *Int. J. Environ. Health Res.* (2023) 1–13.
- G. Yu, A. Tzouveleki, R. Wang, J.D. Herazo-Maya, G.H. Ibarra, A. Srivastava, J.P. W. de Castro, G. Deluiliis, F. Ahangari, T. Woolard, N. Aurelien, E.D.R. Arrojo, Y. Gan, M. Graham, X. Liu, R.J. Homer, T.S. Scanlan, P. Mannam, P.J. Lee, E. L. Herzog, A.C. Bianco, N. Kaminski, Thyroid hormone inhibits lung fibrosis in mice by improving epithelial mitochondrial function, *Nat. Med.* 24 (1) (2018) 39–49.
- C. He, J.L. Larson-Casey, D. Davis, V.S. Hanumanth, A.L.F. Longhini, V. J. Thannickal, L. Gu, A.B. Carter, NOX4 modulates macrophage phenotype and mitochondrial biogenesis in asbestosis, *JCI Insight* 4 (16) (2019).
- S.U. Hettiarachchi, Y.H. Li, J. Roy, F. Zhang, E. Puchulu-Campanella, S. D. Lindeman, M. Srinivasarao, K. Tsoyi, X. Liang, E.A. Ayaub, C. Nickerson-Nutter, I.O. Rosas, P.S. Low, Targeted inhibition of PI3 kinase/mTOR specifically in fibrotic lung fibroblasts suppresses pulmonary fibrosis in experimental models, *Sci. Transl. Med.* 12 (567) (2020).
- S. Du, C. Li, Y. Lu, X. Lei, Y. Zhang, S. Li, F. Liu, Y. Chen, D. Weng, J. Chen, Dioscin alleviates crystalline silica-induced pulmonary inflammation and fibrosis through promoting alveolar macrophage autophagy, *Theranostics* 9 (7) (2019) 1878–1892.
- J.L. Larson-Casey, J.S. Deshane, A.J. Ryan, V.J. Thannickal, A.B. Carter, Macrophage Akt1 kinase-mediated mitophagy modulates apoptosis resistance and pulmonary fibrosis, *Immunity* 44 (3) (2016) 582–596.
- M. Bueno, J. Calyeca, M. Rojas, A.L. Mora, Mitochondria dysfunction and metabolic reprogramming as drivers of idiopathic pulmonary fibrosis, *Redox Biol.* 33 (2020), 101509.
- P.P. Ogger, A.J. Byrne, Macrophage metabolic reprogramming during chronic lung disease, *Mucosal Immunol.* 14 (2) (2021) 282–295.
- M.P. Cervantes-Silva, S.L. Cox, A.M. Curtis, Alterations in mitochondrial morphology as a key driver of immunity and host defence, *EMBO Rep.* 22 (9) (2021), e53086.
- D. Bhatia, A. Capili, K. Nakahira, T. Muthukumar, L.K. Torres, A.M.K. Choi, M. E. Choi, Conditional deletion of myeloid-specific mitofusin 2 but not mitofusin 1 promotes kidney fibrosis, *Kidney Int.* 101 (5) (2022) 963–986.
- J.L. Larson-Casey, C. He, A.B. Carter, Mitochondrial quality control in pulmonary fibrosis, *Redox Biol.* 33 (2020), 101426.
- L. Simula, M. Campanella, S. Campello, Targeting Drp1 and mitochondrial fission for therapeutic immune modulation, *Pharmacol. Res.* 146 (2019), 104317.
- A.A. Rosdah, W.J. Smiles, J.S. Oakhill, J.W. Scott, C.G. Langendorf, L.M. D. Delbridge, J.K. Holien, S.Y. Lim, New perspectives on the role of Drp1 isoforms in regulating mitochondrial pathophysiology, *Pharmacol. Ther.* 213 (2020), 107594.
- G. Zhao, K. Cao, C. Xu, A. Sun, W. Lu, Y. Zheng, H. Li, G. Hong, B. Wu, Q. Qiu, Z. Lu, Crosstalk between mitochondrial fission and oxidative stress in paraquat-induced apoptosis in mouse alveolar type II cells, *Int. J. Biol. Sci.* 13 (7) (2017) 888–900.
- W. Yu, X. Wang, J. Zhao, R. Liu, J. Liu, Z. Wang, J. Peng, H. Wu, X. Zhang, Z. Long, D. Kong, W. Li, C. Hai, Stat2-Drp1 mediated mitochondrial mass increase is necessary for pro-inflammatory differentiation of macrophages, *Redox Biol.* 37 (2020), 101761.
- L. Gu, J.L. Larson-Casey, A.B. Carter, Macrophages utilize the mitochondrial calcium uniporter for profibrotic polarization, *Faseb. J.* 31 (7) (2017) 3072–3083.
- C. Duan, L. Kuang, X. Xiang, J. Zhang, Y. Zhu, Y. Wu, Q. Yan, L. Liu, T. Li, Drp1 regulates mitochondrial dysfunction and dysregulated metabolism in ischemic injury via Clec16a-, BAX-, and GSH- pathways, *Cell Death Dis.* 11 (4) (2020) 251.
- D.K. Jeppesen, A.M. Fenix, J.L. Franklin, J.N. Higginbotham, Q. Zhang, L. J. Zimmerman, D.C. Liebler, J. Ping, Q. Liu, R. Evans, W.H. Fissell, J.G. Patton, L. H. Rome, D.T. Burnette, R.J. Coffey, Reassessment of exosome composition, *Cell* 177 (2) (2019) 428–445 e18.
- M. Hu, Y. Wang, Z. Liu, Z. Yu, K. Guan, M. Liu, M. Wang, J. Tan, L. Huang, Hepatic macrophages act as a central hub for relaxin-mediated alleviation of liver fibrosis, *Nat. Nanotechnol.* 16 (4) (2021) 466–477.
- Z. Wang, K.D. Popowski, D. Zhu, B.L. de Juan Abad, X. Wang, M. Liu, H. Lutz, N. De Naeyer, C.T. DeMarco, T.N. Denny, P.C. Dinh, Z. Li, K. Cheng, Exosomes decorated with a recombinant SARS-CoV-2 receptor-binding domain as an inhalable COVID-19 vaccine, *Nat. Biomed. Eng.* 6 (7) (2022) 791–805.
- K.D. Popowski, A. Moatti, G. Scull, D. Silkstone, H. Lutz, B. Lopez de Juan Abad, A. George, E. Belcher, D. Zhu, X. Mei, X. Cheng, M. Cislo, A. Ghodsi, Y. Cai, K. Huang, J. Li, A.C. Brown, A. Greenbaum, P.C. Dinh, K. Cheng, Inhalable dry powder mRNA vaccines based on extracellular vesicles, *Matter* 5 (9) (2022) 2960–2974.
- K. Dooley, R.E. McConnell, K. Xu, N.D. Lewis, S. Haupt, M.R. Younis, S. Martin, C. L. Sia, C. McCoy, R.J. Moniz, O. Burenkova, J. Sanchez-Salazar, S.C. Jang, B. Choi, R.A. Harrison, D. Houde, D. Burzyn, C. Leng, K. Kirwin, N.L. Ross, J.D. Finn, L. Gaidukov, K.D. Economides, S. Estes, J.E. Thornton, J.D. Kulman, S. Sathyanarayanan, D.E. Williams, A versatile platform for generating engineered extracellular vesicles with defined therapeutic properties, *Mol. Ther.* 29 (5) (2021) 1729–1743.
- W.C. Zhou, J. Qu, S.Y. Xie, Y. Sun, H.W. Yao, Mitochondrial dysfunction in chronic respiratory diseases: implications for the pathogenesis and potential therapeutics, *Oxid. Med. Cell. Longev.* 2021 (2021), 5188306.
- J. Mondal, S. Pillarisetti, V. Junnuthula, M. Saha, S.R. Hwang, I.K. Park, Y.K. Lee, Hybrid exosomes, exosome-like nanovesicles and engineered exosomes for therapeutic applications, *J. Contr. Release* 353 (2022) 1127–1149.
- M. Liu, B. Lopez de Juan Abad, K. Cheng, Cardiac fibrosis: myofibroblast-mediated pathological regulation and drug delivery strategies, *Adv. Drug Deliv. Rev.* 173 (2021) 504–519.
- M. Fairhead, G. Veggiani, M. Lever, J. Yan, D. Mesner, C.V. Robinson, O. Dushek, P.A. van der Merwe, M. Howarth, SpyAvidin hubs enable precise and ultrastable orthogonal nanoassembly, *J. Am. Chem. Soc.* 136 (35) (2014) 12355–12363.
- L. Martinez-Pomares, The mannose receptor, *J. Leukoc. Biol.* 92 (6) (2012) 1177–1186.
- S. Mahalanobish, S. Saha, S. Dutta, P.C. Sil, Matrix metalloproteinase: an upcoming therapeutic approach for idiopathic pulmonary fibrosis, *Pharmacol. Res.* 152 (2020), 104591.
- A. Menou, J. Duitman, B. Crestani, The impaired proteases and anti-proteases balance in Idiopathic Pulmonary Fibrosis, *Matrix Biol.* 68–69 (2018) 382–403.
- L. Gu, J.L. Larson Casey, S.A. Andrabi, J.H. Lee, S. Meza-Perez, T.D. Randall, A. B. Carter, Mitochondrial calcium uniporter regulates PGC-1 α expression to mediate metabolic reprogramming in pulmonary fibrosis, *Redox Biol.* 26 (2019), 101307.
- H.L. Osborn-Heaford, A.J. Ryan, S. Murthy, A.M. Racila, C. He, J.C. Sieren, D. R. Spitz, A.B. Carter, Mitochondrial Rac1 GTPase import and electron transfer from cytochrome c are required for pulmonary fibrosis, *J. Biol. Chem.* 287 (5) (2012) 3301–3312.
- H.P. Indo, M. Davidson, H.C. Yen, S. Suenaga, K. Tomita, T. Nishii, M. Higuchi, Y. Koga, T. Ozawa, H.J. Majima, Evidence of ROS generation by mitochondria in cells with impaired electron transport chain and mitochondrial DNA damage, *Mitochondrion* 7 (1–2) (2007) 106–118.
- X.N. An, Z.N. Wei, Y.Y. Xie, J. Xu, Y. Shen, L.Y. Ni, H. Shi, P.Y. Shen, W. Zhang, Y. X. Chen, CD206(+)CD68(+) mono-macrophages and serum soluble CD206 level are increased in antineutrophil cytoplasmic antibodies associated glomerulonephritis, *BMC Immunol.* 23 (1) (2022) 55.
- J. Glaubitz, A. Wilden, J. Golchert, G. Homuth, U. Volker, B.M. Broker, T. Thiele, M.M. Lerch, J. Mayerle, A.A. Aghdassi, F.U. Weiss, M. Sandler, In mouse chronic pancreatitis CD25(+)FOXP3(+) regulatory T cells control pancreatic fibrosis by suppression of the type 2 immune response, *Nat. Commun.* 13 (1) (2022) 4502.
- J. Zou, M. Shi, X. Liu, C. Jin, X. Xing, L. Qiu, W. Tan, Aptamer-functionalized exosomes: elucidating the cellular uptake mechanism and the potential for cancer-targeted chemotherapy, *Anal. Chem.* 91 (3) (2019) 2425–2430.
- J. Yang, S. Wu, L. Hou, D. Zhu, S. Yin, G. Yang, Y. Wang, Therapeutic effects of simultaneous delivery of nerve growth factor mRNA and protein via exosomes on cerebral ischemia, *Mol. Ther. Nucleic Acids* 21 (2020) 512–522.
- H. Kim, N. Yun, D. Mun, J.Y. Kang, S.H. Lee, H. Park, H. Park, B. Joung, Cardiac-specific delivery by cardiac tissue-targeting peptide-expressing exosomes, *Biochem. Biophys. Res. Commun.* 499 (4) (2018) 803–808.
- Z. Deng, M.W. Fear, Y. Suk Choi, F.M. Wood, A. Allahham, S.E. Mutsaers, C. M. Prele, The extracellular matrix and mechanotransduction in pulmonary fibrosis, *Int. J. Biochem. Cell Biol.* 126 (2020), 105802.
- G. Yu, E. Kovkarova-Naumovski, P. Jara, A. Parwani, D. Kass, V. Ruiz, C. Lopez-Otin, I.O. Rosas, K.F. Gibson, S. Cabrera, R. Ramirez, S.A. Yousem, T.J. Richards, L. J. Chensny, M. Selman, N. Kaminski, A. Pardo, Matrix metalloproteinase-19 is a key regulator of lung fibrosis in mice and humans, *Am. J. Respir. Crit. Care Med.* 186 (8) (2012) 752–762.
- P.C. Dinh, D. Paudel, H. Brochu, K.D. Popowski, M.C. Gracieux, J. Cores, K. Huang, M.T. Hensley, E. Harrell, A.C. Vandergriff, A.K. George, R.T. Barrio, S. Hu, T.

- A. Allen, K. Blackburn, T.G. Caranasos, X. Peng, L.V. Schnabel, K.B. Adler, L. J. Lobo, M.B. Goshe, K. Cheng, Inhalation of lung spheroid cell secretome and exosomes promotes lung repair in pulmonary fibrosis, *Nat. Commun.* 11 (1) (2020) 1064.
- [45] N. Joshi, S. Watanabe, R. Verma, R.P. Jablonski, C.I. Chen, P. Cheres, N. S. Markov, P.A. Reyfman, A.C. McQuattie-Pimentel, L. Sichizya, Z. Lu, R. Piseaux-Aillon, D. Kirchenbuechler, A.S. Flozak, C.J. Gottardi, C.M. Cuda, H. Perlman, M. Jain, D.W. Kamp, G.R.S. Budinger, A.V. Misharin, A spatially restricted fibrotic niche in pulmonary fibrosis is sustained by M-CSF/M-CSFR signalling in monocyte-derived alveolar macrophages, *Eur. Respir. J.* 55 (1) (2020).
- [46] T. Guo, C.S. Jiang, S.Z. Yang, Y. Zhu, C. He, A.B. Carter, V.B. Antony, H. Peng, Y. Zhou, Mitochondrial fission and bioenergetics mediate human lung fibroblast durotaxis, *JCI Insight* 8 (1) (2023).
- [47] N. Hieta, U. Impola, C. Lopez-Otin, U. Saarialho-Kere, V.M. Kahari, Matrix metalloproteinase-19 expression in dermal wounds and by fibroblasts in culture, *J. Invest. Dermatol.* 121 (5) (2003) 997–1004.
- [48] J. Prieto, M. Leon, X. Ponsoda, R. Sendra, R. Bort, R. Ferrer-Lorente, A. Raya, C. Lopez-Garcia, J. Torres, Early ERK1/2 activation promotes DRP1-dependent mitochondrial fission necessary for cell reprogramming, *Nat. Commun.* 7 (2016), 11124.
- [49] X. Zhang, R. Goncalves, D.M. Mosser, The isolation and characterization of murine macrophages, *Curr Protoc Immunol Chapter 14* (2008) 14 1 1–14 1 14.
- [50] W.O. Carter, P.K. Narayanan, J.P. Robinson, Intracellular hydrogen peroxide and superoxide anion detection in endothelial cells, *J. Leukoc. Biol.* 55 (2) (1994) 253–258.